Journal of ELECTRONIC MATERIALS, Vol. 45, No. 9, 2016
DOI: 10.1007/s11664-016-4738-4

Opto-electronic Properties of Mid-Wavelength: n Type II InAs/$InAs_{1-x}Sb_x$ and $Hg_{1-x}Cd_xTe$

ROGER E. DE WAMES[1,2]

1.—Fulcrum Co., Centerville, VA 20120, USA. 2.—e-mail: rdewames@gmail.com

There is significant interest in mid-wavelength type II strained layer superlattices (SLSs) and HgCdTe material systems for background limited performance, operating at significantly higher temperature, $T \geq 150$ K, than InSb, $T \approx 80$–90 K. A precise knowledge of the electronic and optical properties of these materials is desirable since they determine detector performance and are needed for input parameters in self-consistent physics-based predictive models. Recently, data on the optical absorption coefficient, and the hole minority carrier lifetime has become available, suggesting that in the extrinsic region the limiting recombination processes in mid-wavelength type II Ga-free SLSs are radiative and Shockley–Read–Hall (SRH). These findings provide the opportunity for comparisons with mid-wavelength HgCdTe. The comparisons show that the radiative recombination coefficients are similar; however, the SRH lifetime limited to 9 μs for the SLS implies that the dark current density is expected to be limited by bulk generation–recombination (G–R) SRH processes for temperatures below 160 K; hence requiring heterojunction designs to suppress the G–R dark currents and be diffusion limited. Mid-wavelength infrared HgCdTe photodiodes are shallow p^+n photovoltaic devices and because of the very long SRH hole lifetime are diffusion radiatively limited photodiodes down to 80 K.

Key words: Heterojunctions, superlattices, InAsSb, HgCdTe, infrared detectors

INTRODUCTION

In contrast to binary mid-wavelength infrared (MWIR) InAs/GaSb p-type II superlattices, which are limited in detector performance by relatively low electron minority Shockley–Read–Hall (SRH) lifetimes ~80 ns, recently published MWIR Ga free n-type II (43 Å, 12 Å)—$InAs/InAs_{0.54}Sb_{0.46}$ structures have much longer lifetimes ~4.5 μs at 77 K, $\tau_{rad.} \sim 8$ μs, and $\tau_{SRH} = 10$ μs.[1] For the samples reported, the n-type carrier concentration was estimated from capacitance to voltage measurements to be $\sim 5 \times 10^{14}$ cm^{-3}. The strained layer superlattice (SLS) samples were double heterostructures with InAs/InAsSb sandwiched between two 60 nm thick $AlAs_{0.08}Sb_{0.92}$ layers. Optical absorption spectroscopy was used to measure the absorption coefficient α (cm^{-1}). The energy gap was determined using photoluminescence (PL) and the recombination lifetime measurements were made using the optical modulation response method. Based on the observation that the intrinsic recombination lifetime in the extrinsic region of the semiconductor is dominated by radiative recombination and not Auger(e–e) processes,[1,2] the spectral shape and position of the absorption edge is important to quantify.[3] From the absorption edge the energy gap can be determined and from the spectral absorption the radiative recombination rate per unit volume G_r (cm^{-3} s^{-1}) can be calculated.[4] At a given temperature, G_r and n_i, the intrinsic carrier concentration, are fixed, and the radiative lifetime is given by $\tau_{rad} = n_i^2/[G_r(n_0 + p_0)]$. The radiative recombination coefficient B (cm^3 s^{-1}) is defined as G_r/n_i^2. Hence, the radiative lifetime depends on the doping when the

(Received December 6, 2015; accepted June 7, 2016; published online June 29, 2016)

excess carrier concentration $n_e \ll (n_0 + p_0)$, with n_0 and p_0 the equilibrium electron and hole concentrations, respectively. To calculate $B(T, E_g)$, given $E_g(T)$ from the (PL) data, an estimate of the electron and hole effective masses was used to calculate $n_i(T)$. A series of absorption spectra at selected temperatures were measured[1,2] to calculate $G_r(T)$. This methodology to interpret the measured recombination lifetime provided a fit to the data with the SRH recombination lifetime and photon recycling factor as fitting parameters.[1,2] In our analysis, using the measured spectral absorption coefficients we derive analytical equations for the radiative recombination coefficient $B(T, E_g)$ that enables a functional comparison on temperature and energy gap with $B(T, E_g)$ for MWIR HgCdTe.[5] The analysis provides the Varshni parameters for this SLS structure energy gap as a function of temperature and $E_g(0\ \text{K})$,[6] and a prediction of the dark current density as a function of the detector operating temperature.

The manuscript is organized as follows: in "Radiative Recombination Coefficients for SLS and HgCdTe" section we compare the radiative recombination coefficient $B(T, E_g)$ for the SLS and HgCdTe. In "Measured and Modeled Recombination Lifetime" section we model the recombination lifetime measured.[1] "Modeled MWIR InAs/InAsSb Dark Current Density" section contains a calculation of the expected dark current density for the SLS as a function of the inverse temperature of the detector. "MWIR HgCdTe Measured and Modeled Dark Current Density" section contains the measured dependence of the recombination lifetime at 80 K for mid-wavelength HgCdTe on the donor carrier concentration N_d (cm^{-3}), including discussions on the modeled and measured focal plane array dark current density data as a function of inverse temperature.[7] The summary including suggestions for future research directions are presented in "Summary and Research Needs" section. Section VII contains the acknowledgements and section VIII contains the references.

RADIATIVE RECOMBINATION COEFFICIENTS FOR SLS AND HGCDTE

In Fig. 1, we show the measured optical absorption coefficient spectral shape and position of the band edge used to determine the energy gap at 77 K. The data was fitted below the gap with the Urbach expression shown in the insert and above the gap with a functional equation on the photon energy and energy gap for a direct band gap semiconductor. The fit is observed to be good for energy above the gap $\sim 10kT$, which is the region that contributes the most to the integral equation for the recombination rate per unit volume given by[4]

$$G_r = 8\pi h^{-3}(n/c)^2 \int \{\alpha(E)E^2/[\exp(E/kT) - 1]\}\mathrm{d}E, \quad (1)$$

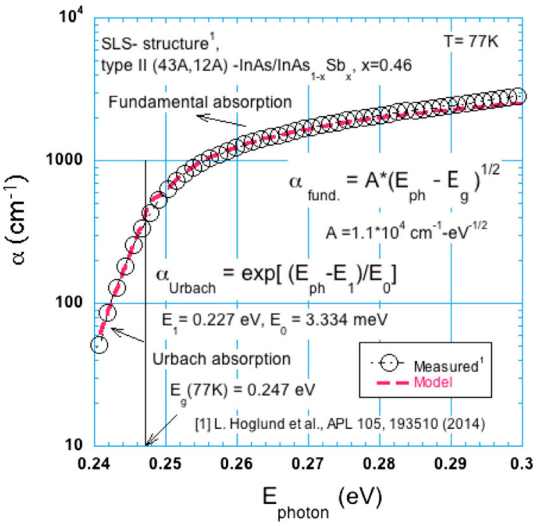

Fig. 1. Optical absorption coefficient versus photon energy of a type II mid-wavelength InAs/InAsSb superlattice.

where n is the index of refraction, h Plank constant, and $\alpha(E)$ is the spectral absorption coefficient in cm^{-1}.

Figure 2, is a plot of Plank equation for Q_{eq} the number of photons per unit volume in a range $\mathrm{d}\nu$ as a function of photon energy. Shown is the absorption coefficient and the product αQ_{eq} with photon energy. The area under the curve αQ_{eq} provided the value of $G_r(77\ \text{K})$ given in the insert. The Q_{eq} dependence on photon energy clearly illustrates that the exponential term in the Plank expression is dominant in the region of integration, this behavior is attributed to the value of the band gap energy that is much higher than kT in this region.

A series of measured spectral optical absorption coefficients in the temperature range 77–275 K were provided[8] that enabled using the analysis described for the case $T = 77$ K to construct the Table I containing important information on the material properties for the SLS structure (43 Å, 12 Å) $\text{InAs/InAs}_{1-x}\text{Sb}_x$, $x = 0.46$, superlattice.[1]

G_r: radiative recombination rate per unit volume is calculated from the measured optical absorption coefficient[1] in cm^{-1}, as well as the band gap energy $E_g(T) = E_g(0) - \alpha T^2/(T + \beta)$, where $E_g(0) = 0.2533$ eV, $\alpha = 3.9384 \times 10^{-4}$ eV K^{-1}, $\beta = 295.52$ K. $B(T)$ the radiative recombination coefficient $= G_r/n_i^2$. $N_d = 5 \times 10^{14}$ cm^{-3}. $m_v/m_0 = 0.368$, $m_c/m_0 = 0.0274$. The effective mass, for the conduction and valence band, which enabled the calculation of $n_i(T)$ was provided by Dr. Dave Ting. The table contains the calculation of the Auger recombination lifetime; this topic is discussed in "Measured and Modeled Recombination Lifetime" section.

Figure 3, is a plot of the radiative recombination coefficient as a function of the inverse temperature calculated from the numerical integration of integral for G_r, Eq. 1 The empirical fit to the data is given by $B = m_1/T^{m2}$, hence the radiative lifetime

$\tau_{\text{rad.}} = T^{m2}/(m_1 \times N_d)$, when $n_{n0} = N_d$ and $p_{n0} = n_i^2/N_d$, valid for temperatures < 175 K.

It is useful to derive an analytical equation for G_r, and hence B to compare with previously derived expressions for MWIR HgCdTe and analytical expressions for the functional dependence on temperature and the band gap energy $E_g(T)$. G_r as a functional dependence of the form $\exp(-E_g/kT)$, similarly $n_i^2(T) \sim \exp(-E_g/kT)$, hence $B = G_r/n_i^2$ is expected to have a polynomial dependence on E_g, consequently SLS samples with comparable energy gaps and absorption coefficients would be expected to have basically the same radiative recombination coefficient; a useful result for the analysis of comparable SLS structure designs.

Using for the spectral absorption coefficient the equation $\alpha(E) = A(T) \times (E - E_g)^{1/2}$, where $A(T)$ is observed to be essentially a constant for the SLS structure and equal to 1.1×10^4 cm^{-1} eV$^{-1/2}$, the integral Eq. 1 for G_r becomes,

$$G_r = 8\pi h^{-3}(n/c)^2 A(T) \times \int (E - E_g)^{1/2} E^2 \exp(-E/kT)\,dE, \tag{2}$$

where the lower limit to the integral is E_g and the upper limit ∞.

Changing the variable of integration so that the lower limit is zero, Eq. 2 becomes

$$\begin{aligned} G_r &= \text{Const.} A(T) \times (kT)^{7/2} \times \exp(-E_g/kT) \\ &\quad \times \Gamma_r(E_g/kT), \\ \text{Const.} &= 8\pi h^{-3}(n/c)^2 = 4.844 \times 10^{24}, \\ n &= 3.51, \quad c = 3 \times 10^{10} \text{ cm s}^{-1}, \\ h &= 4.1414 \times 10^{-15} \text{ eV s}, \end{aligned} \tag{3}$$

$$\Gamma_r(E_g/kT) = \Gamma_{r1} + 2(E_g/kT)\Gamma_{r2} + (E_g/kT)^2 \Gamma_{r3}, \tag{4}$$

where $\Gamma_{r1} = \int x^{5/2} e^{-x} dx$, $\Gamma_{r2} = \int x^{3/2} e^{-x} dx$, $\Gamma_{r3} = \int x^{1/2} e^{-x} dx$.

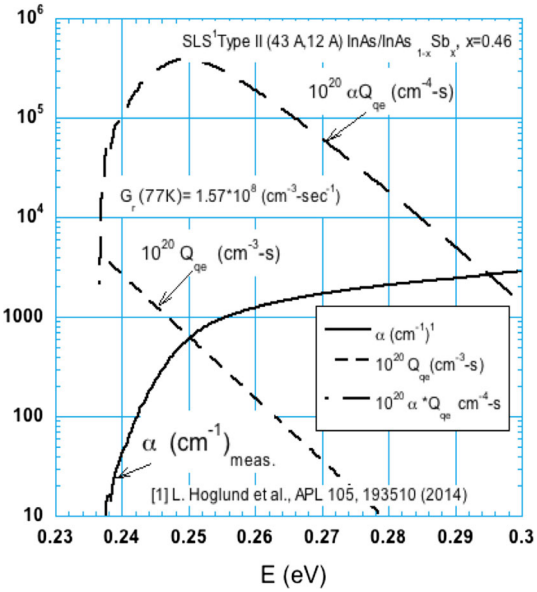

Fig. 2. Variations of Q_{eq}, α, and their product with photon energy for 77 K black body radiation.

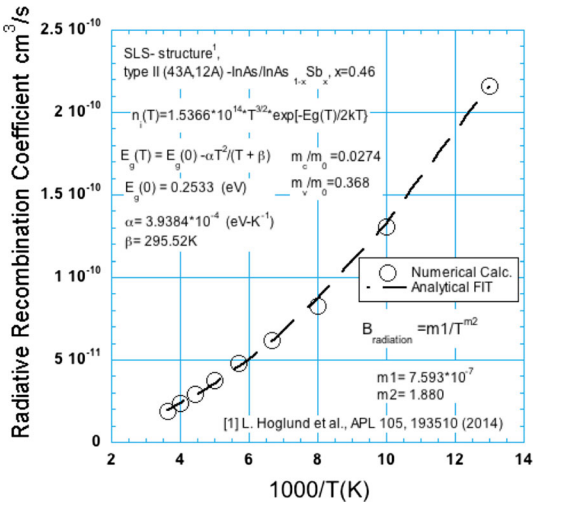

Fig. 3. Radiative recombination coefficient versus inverse temperature for a type II mid-wavelength InAs/InAsSb superlattice.

Table I. Properties of a mid-wavelength n type II (43 Å, 12 Å) InAs/InAs$_{1-x}$Sb$_x$, x = 0.46, superlattice

T (K)	$E_g(T)$ (eV)	$n_i(T)$ (cm^{-3})	τ_{Auger} μs $F_1F_2 = 0.22$	G_r-rad. recom. rate (cm^{-3} s^{-1})	B-rad. recom. coeff. (cm^3 s^{-1})	$\tau_{\text{rad.}}$ $1/(BN_d)$ (μs)
77	0.2471	8.531×10^{8}	170.74	1.570×10^{8}	2.16×10^{-10}	9.27
100	0.2434	1.132×10^{11}	132.51	1.674×10^{12}	1.31×10^{-10}	15.31
125	0.2387	3.312×10^{12}	118.01	9.064×10^{14}	8.27×10^{-11}	24.20
150	0.2334	3.381×10^{13}	111.42	7.045×10^{16}	6.16×10^{-11}	32.46
175	0.2277	1.873×10^{14}	79.470	1.692×10^{18}	4.83×10^{-11}	33.17
200	0.2215	7.029×10^{14}	18.858	1.861×10^{19}	3.77×10^{-11}	17.80
225	0.2150	2.026×10^{15}	3.024	1.208×10^{20}	2.94×10^{-11}	8.32
250	0.2082	$4.840 \times 10^{1.5}$	0.579	5.461×10^{20}	2.33×10^{-11}	4.43
275	0.2011	1.006×10^{16}	0.2011	1.867×10^{21}	1.85×10^{-11}	2.69

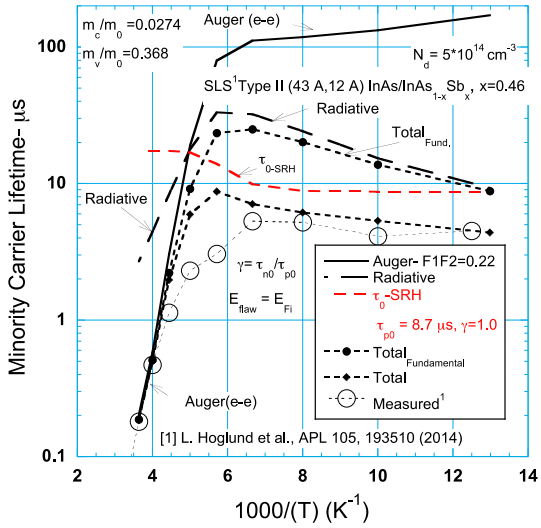

Fig. 4. Minority carrier lifetime versus inverse temperature for a n-type II mid-wavelength InAs/InAsSb superlattice.

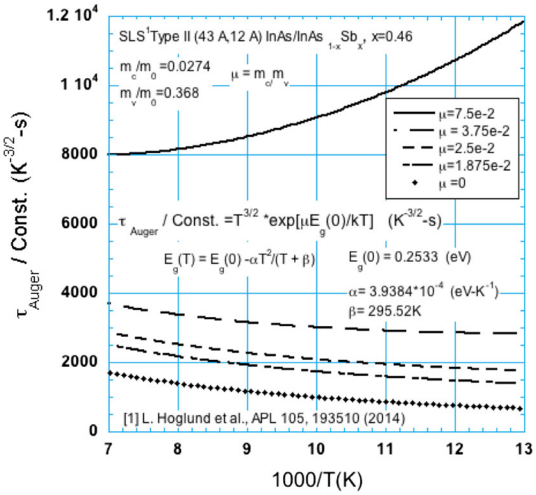

Fig. 5. Auger minority carrier lifetime versus inverse temperature for a mid-wavelength InAs/InAsSb superlattice: $\mu = m_c/m_v$ as a parameter.

These integrals are related to Gamma functions as shown:[9]

$$\Gamma_{r1} = \Gamma(7/2) = 3.32335,$$
$$\Gamma_{r2} = \Gamma(5/2) = 1.32934,$$
$$\Gamma_{r3} = \Gamma(3/2) = 0.88623.$$

Inserting the above numbers into Eq. 4 we obtain

$$\Gamma_r(E_g/kT) = 0.88623 \times \left\{ [E_g(T)/kT]^2 + 3[E_g(T)/kT] + 3.75 \right\}, \quad (5)$$

$$G_r = 3.444 \times 10^{18} \times A(T) \times T^{3/2} \times \exp(-E_g/kT) \times \left\{ [E_g(T)]^2 + 3[(kT)E_g(T)] + 3.75(kT)^2 \right\} \ (\mathrm{cm}^{-3}\ \mathrm{s}^{-1}). \quad (6)$$

Using the above expression for G_r and the equation for $n_i(T) = 1.5366 \times 10^{14} \times T^{3/2} \times \exp[-E_g(T)/kT]$, we obtain

$$B(T) = G_r/n_i^2 = 2.8 \times 10^{-14} \times A(T) \times (300/T)^{3/2} \times \left\{ [E_g(T)]^2 + 3[(kT)E_g(T)] + 3.75(kT)^2 \right\}. \quad (7)$$

Hence, while the recombination rate G_r and the intrinsic carrier concentration has an exponential dependence on the energy gap at a fixed temperature, the radiative recombination coefficient is a polynomial of second degree. Hence, structures with similar band gaps are expected to have basically the same B value.

The radiative recombination for HgCdTe is given by[5]

$$B(T) = 5.8 \times 10^{-13} \times \sqrt{\varepsilon_\infty} \times [1/(m_c/m_0 + m_v/m_0)]^{3/2} \times [1 + 1/(m_c/m_0) + 1/(m_v/m_0)] \times (300/T)^{3/2} \times \left\{ [E_g(T)]^2 + 3[(kT)E_g(T)] + 3.75(kT)^2 \right\}, \quad (8)$$

where $m_c/m_0 = 1/\{-0.6 + 6.333 \times [2/E_g(T) + 1/(E_g(T) + 1)]\}^{10} \approx E_g(T)/13$, $m_v/m_0 = 0.5$, and ε_∞ is the relative high frequency dielectric constant [11]. (9)

An interesting observation in comparing the two equations is that the term $(300/T)^{3/2} \times \{[E_g(T)]^2 + 3[(kT)E_g(T)] + 3.75(kT)^2\}$, is common to the two expressions.

The pre-factor $A(T)$ in Eq. 7 is observed to be a constant equal to $1.1 \times 10^4\ \mathrm{cm}^{-1}\ \mathrm{eV}^{-1/2}$, hence the pre-factor of $B(T)$ is 3.1×10^{-10}. The SLS structure (43 Å, 12 Å) InAs/$InAs_{1-x}Sb_x$, $x = 0.46$, superlattice[1] at 77 K has a band gap of 0.2471 eV; this corresponds to $x = 0.3025$ in the chemical formula $Hg_{1-x}Cd_xTe$. For this case,[10] $m_c/m_0 = 0.01794$, $m_v/m_0 = 0.5$, $\varepsilon_\infty = 11.64$, and the pre-factor of $B(77\ \mathrm{K}) = 3.1 \times 10^{-10}$. Deviations are expected as a function of temperature, since for HgCdTe, $x = 0.3025$ the band gap energy $E_g(T) = 0.2305 + 2.113 \times 10^{-4} \times T$, increasing with temperature, whereas for the SLS structure, $E_g(T) = 0.2533 - 3.9384 \times 10^{-4} \times T^2/(T + 295.52\ \mathrm{K})$ decreasing with temperature.

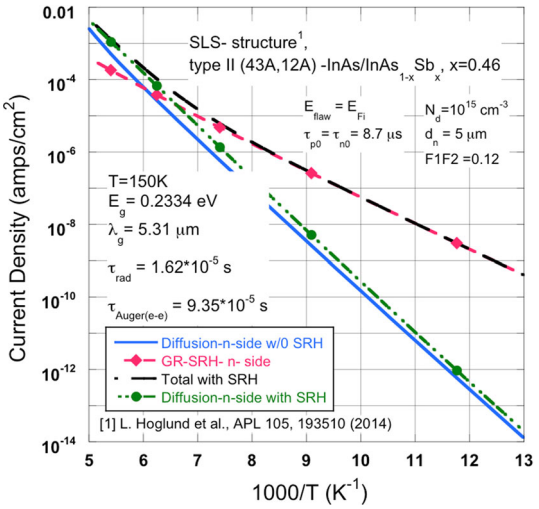

Fig. 6. MWIR InAs/InAsSb modeled current density versus inverse temperature, $V_{bias} = -250$ mV.

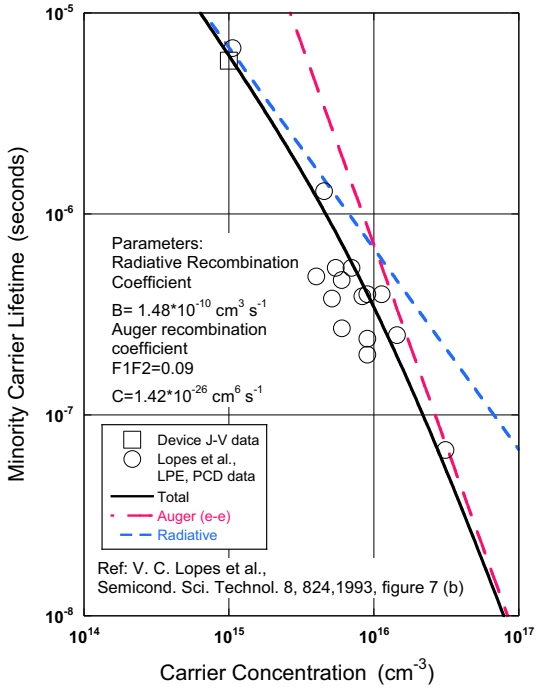

Fig. 7. Measured and modeled minority carrier lifetime as a function of carrier concentration for MWIR n-type Hg$_{1-x}$Cd$_x$Te, $x = 0.3$ materials, $T = 80$ K. $N_d = 10^{15}$ cm^{-3}, $\tau_{rad.} = 6.76$ μs, $F_1F_2 = 0.09$, $\tau_{Auger} = 70.4$ μs, $\tau_{Total} = 6.2$ μs, $B = 1.48 \times 10^{-10}$ cm^3 s^{-1}, $C = 1.42 \times 10^{-26}$ cm^6 s^{-1}.

From the above considerations and results, it is concluded that in the case the fundamental limiting recombination mechanism is radiative both material systems are expected to have the same dark current density; taking into considerations that $E_g(T)$ for MWIR HgCdTe increases with temperature, whereas it decreases for the type II SLS III–V materials.

MEASURED AND MODELED RECOMBINATION LIFETIME

In Fig. 4 the measured and modeled hole minority carrier lifetime is plotted as a function of inverse temperature. In the extrinsic region ($n_{n0} = N_d > n_i > p_{n0}$), the lifetime is dominated by the SRH hole lifetime τ_{p0} determined by setting at 77 K $\tau_{meas.} = \tau_{rad.} \times \tau_{p0}/(\tau_{rad.} + \tau_{p0})$. Taking the measured lifetime to be 4.5 μs and the radiative lifetime of 9.3 μs the calculated τ_{p0} lifetime is 8.7 μs. In this simulation the position of the flaw energy in the forbidden gap is $E_{flaw} = E_{Fi}$, where E_{Fi} is the intrinsic Fermi level. In this simulation only the SRH lifetime was used as a fitting parameter. The SRH lifetime in[1] was estimated to be 10 μs. For the condition that $\tau_{n0} = \tau_{p0}$ the temperature dependence of τ_0 the SRH lifetime for n-type materials is given by the expression $\tau_0 = \tau_{p0}[1 + 2n_i/(n_{n0} + p_{n0})]$[4]. As shown in the figure the behavior is a constant in the extrinsic region and increases to a value of $2\tau_{p0}$ in the intrinsic region, $T \geq 200$ K. In the intrinsic region the dominant recombination mechanism is Auger(e–e). However, in the extrinsic region the dominant recombination mechanisms are radiative and SRH, assuming the SRH lifetime does not depend on carrier concentration, for higher doping condition the radiative processes are expected to become dominant.[2]

Noteworthy is the behavior of the Auger(e–e) in the extrinsic region of the semiconductor. This behavior is attributed to the observation that the Auger lifetime $\tau_{Auger} = \text{Const.} \times T^{3/2} \times \exp\{[\mu/(1 + \mu)]E_g(0)/kT\}$, where $\mu = m_e/m_v < 1$.[4]

In Fig. 5 the dependence of the Auger lifetime in the extrinsic region as a function of the inverse temperature is shown for various values of μ for the mid-wavelength n type II (43 Å, 12 Å) InAs/InAs$_{1-x}$Sb$_x$, $x = 0.46$, superlattice. As expected, from the expression for the Auger lifetime the dependence is sensitive to the exponent $\{[\mu/(1 + \mu)]E_g(0)/kT\}$. For mid-wavelength Hg$_{1-x}Cd_x$Te, $x = 0.3025$, $\mu = 3.59 \times 10^{-2}$ and $E_g(0) = 0.2305$ eV. Hence, we expect a decrease of the Auger lifetime in the extrinsic region.

The solid black dots label total fundamental include in the calculation the radiative and Auger recombination lifetimes. The diamond (black) symbol label total include the three recombination processes. Radiative, Auger, and SRH. The SRH model assumes that the energy of the flaw E_{flaw} is equal to the intrinsic Fermi energy level E_{Fi}. The electron and hole effective masses are not expected to be strong functions of temperature and taken to be a constant.

MODELED MWIR INAS/INASSB DARK CURRENT DENSITY

The measured bulk minority hole recombination lifetime can be used to determine the bulk

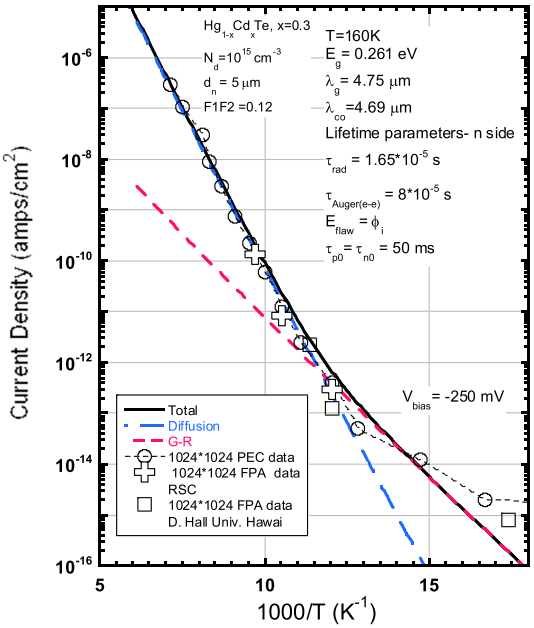

Fig. 8. MWIR photodiode current density versus inverse temperature for very large area devices and FPA data. T = 78 K, x = 0.3, λ_g = 5.1 μm, $\tau_{rad.}$ = 6.15 μs, F_1F_2 = 0.12, τ_{Auger} = 39 μs, τ_{Total} = 5.6 μs.

recombination components, radiative, Auger, and SRH and provide the needed information to predict the dark current density as a function of the inverse temperature. The result of the calculation, assuming that the hole diffusion length L_p is larger than W_n the width of the n-neutral region, is illustrated in Fig. 6. What is evident is that the dominant performance limiting dark current density for the MWIR SLS material is associated with carrier recombination in the depletion region of the n-type material. To be limited by diffusion currents, heterostructure design architectures will be needed in these SLS devices to suppress the generation–recombination (G–R) currents in the n side depletion layer.

The analytical equations used in the calculations of the reverse bias dark current density shown in Fig. 6 are given by

$$J_{\text{d-diffusion-sat-n-side}} = qn_i^2 W_n [B(T) + N_d C(T) + 1/(\tau_{\text{SRH-n}} N_d)], \tag{10}$$

$$J_{\text{GR-SRH}} = -qn_i(T) W_{\text{depletion}}(0) \times \left\{ -V_a + (2/\beta_T) \times \ln\left[1/\Upsilon^{1/2} + \Upsilon^{1/2} \right] \right\} / \left[\tau_\infty V_{bi} (1 - V_a/V_{bi})^{1/2} \right], \tag{11}$$

where $\tau_\infty = \tau_{p0} + \tau_{n0} = \tau_{p0}(1 + \Upsilon)$.

For the condition, γ = 1, Eq. 11 becomes

$$J_{\text{GR-SRH}} = -qn_i(T) \times W_{\text{depletion}}(0) \{ -V_a + (2/\beta_T) \ln(2) \} / \left[2\tau_{p0} V_{bi} (1 - V_a/V_{bi})^{1/2} \right]. \tag{12}$$

Equation (12) for reverse bias voltages greater than V_{bi} becomes

$$J_{\text{GR-SRH}} = -qn_i(T) W_{\text{depletion}}(V_a) / (2\tau_{p0}), \tag{13}$$

T = 150 K, parameters: E_g = 0.2334 eV, n_i = 3.38 × 10^{13} cm^{-3}, $W_n = d_n - W_{\text{depletion-n-side}}(V_a)$ = 4.2 μm, V_a = −0.25 V, d_n = thickness of the n-side absorber region = 5 μm, W_n is the thickness of the n-side neutral region, $N_d = 10^{15}$ cm^{-3}, B = 6.16 × 0^{-11} cm^3/s, F_1F_2 = 0.12, C = 1.062 × 10^{-26} cm^6/s, $\tau_{\text{SRH-n}} = \tau_{p0}(1 + 2n_i/N_d)$, τ_{p0} = 8.7 μs, $\gamma = \tau_{n0}/\tau_{p0}$ = 1, $W_{\text{depletion-n-side}}(0)$ = 0.51 μm, V_{bi} = 0.1476 V, $\beta_T = q/kT$ = 77.363 V^{-1}.

The solid line labeled diffusion-n-side w/o SRH is a calculation of the diffusion dark current that includes both the radiative and Auger recombination processes. The dashed black line labeled total with SRH includes all three recombination processes. The dashed line with dots labeled diffusion-n-side with SRH is a calculation of the diffusion current that includes the SRH recombination processes generated in the neutral region.

MWIR HGCDTE MEASURED AND MODELED DARK CURRENT DENSITY

In Fig. 7 we shown the measured and modeled hole minority carrier lifetime as a function of donor concentration N_d (cm^{-3}).[7]

What is most important about this data and the determination of the dominant recombination mechanisms is the observation that for N_d values in the range of 10^{15} cm^{-3} the dominant process is radiative and that the Auger overlap parameter F_1F_2 is 0.09 for MWIR material and not 0.2 as commonly assumed. In Fig. 8, measured and modeled dark current density as a function of inverse temperature for mid-wave $Hg_{1-x}Cd_xTe$, x = 0.3,[7] is shown. In contrast to the SLS mid-wavelength the dark current density is diffusion limited to temperatures ≈ 80 K. This behavior is due to the very long SRH lifetimes observed in mid-wave HgCdTe.[11]

SUMMARY AND RESEARCH NEEDS

During the past few years, significant investments were made to explore the potential of III–V type II SLS based on the premise that these materials systems could displace HgCdTe for missions requiring imaging in the long wavelength infrared (LWIR) and very LWIR (VLWIR) spectral region. Similar to HgCdTe type II SLS devices offer energy gap tunability from the MWIR to the VLWIR.

Auger recombination is the limiting fundamental recombination mechanism in HgCdTe materials with band gap energy in the LWIR and VLWIR and from theoretical considerations type II SLS could be designed to significantly suppress this intrinsic recombination process. Other considerations dealt with the electron effective mass of both material systems; the effective mass significantly impacts tunneling currents and the larger effective mass for the SLS was expected to reduce significantly tunneling currents. Other anticipated SLS benefits, include expectations of superior overall manufacturability and cost reductions.

However, real SLS-p-type II binary InAs/GaSb superlattices, are limited by SRH centers with electron minority carrier lifetime in the 35–80 ns. For the binary case the band gap state associated with these relatively low SRH lifetime is suspected to be a native Ga defect and hence likely to be difficult to remove. A breakthrough occurred with the observation that the Ga-free ternary alloy type II SLS-n type InAs/InAs$_{(1-x)}$Sb$_x$ exhibited relatively longer lifetimes compared to the binary compounds. In particular, for mid-wave materials the observed limiting lifetime was radiative with SRH lifetime ≈ 10 μs;[1,2] simplicity in the growth of Ga free SLS alloys was an added important benefit.

While the dominant interest and technology challenge is in the development of LWIR and VLWIR materials, and in particular the potential use of the type II InAs/InAsSb alloy, in this paper we compare some of the material properties of mid-wave SLSs with HgCdTe. A notable observation is that both material systems in the extrinsic region of operation $n_{n0} = N_d > n_i > p_{n0}$ are intrinsically limited by radiative recombination and SRH recombination. The method of analysis of the measured hole minority carrier lifetime for this work involved a calculation of G_r (cm^{-3} s^{-1}), the radiative recombination rate per unit volume, made possible by the recent measurements and availability of the optical absorption coefficients data.[1,8] Using this methodology we fitted the recombination lifetime data with only the SRH lifetime as a fitting parameter. We found that both material systems are expected to have similar dark currents when limited by radiative recombination processes. However, the dark current limiting the mid-wave SLS is predicted to originate in the n-side depletion layer for temperatures ≤150 K, while for HgCdTe the observed onset of depletion limiting currents is ≤80 K. For the SLS structure to suppress the depletion dark current for temperatures ≤150 K, it will be necessary to position the n-side absorber depletion layer region in the larger gap cap layer material in a p$^+$n shallow heterostructure detector or barrier layer as commonly practiced in the nBn heterostructure detectors[12] and XBn barrier detectors.[13]

MWIR SLS devices designed to suppress the G–R currents are expected to require the application of reverse bias to collect the diffusion photocurrent generated in the absorber and of course along with the diffusion dark current generated in the absorber; Fig. 6 dashed line with dots labeled diffusion-n-side with SRH.

Sensitivity parameters that influence the bias voltage required to collect the photocurrent generated in the absorber are band gap energy profiles, energy band offsets, composition profiles, carrier type, levels, and profiles in the vicinity of the metallurgical interface and interface states.[14,15] Minority carrier hole lifetime and mobility is expected to be position dependent in the vicinity of the hetero-metallurgical interface.

While the MWIR heterostructure detector concept has been demonstrated,[13] data are still needed on the demonstration of process control over large areas, particularly the capability to produce high quality-large format small pitch focal plane arrays with adequate yield and affordable costs.

To continue to improve LWIR and MWIR SLS device performance, more materials information on the properties of SLS type II alloys is needed, including measurements of the transport properties, mobilities and mechanisms, and diffusion lengths. These material properties for HgCdTe are already known and do not appear to limit the dark current or the quantum efficiency.[16]

Of concern for the LWIR Ga free n-type materials is the observation of relatively low quantum efficiency possibly caused by relatively low optical absorption coefficient, hole mobility, and hence diffusion length.[17] Timely information is now needed on the material/optical, and electronic properties of type II SLS with emphasis on assessing their fundamental and technology material limitations.

ACKNOWLEDGEMENTS

I am very grateful to Dr. Linda Hoglund for providing detail data on the spectral optical absorption coefficient and the recombination lifetime measured at several temperatures in the range 80–275 K; information and helpful discussions that led to the results presented here. I thank Dr. Philip Perconti from the Army Research Laboratory and Dr. Whitney Mason from NVESD for their encouragements and support to try to understand how detectors work to make the needed improvements.

REFERENCES

1. L. Hoglund, D.Z. Ting, A. Soibel, A. Fisher, A. Khoshakhlagh, C.J. Hill, S. Keo, and S.D. Gunapala, *Appl. Phys. Lett.* 105, 193510 (2014).
2. L. Hoglund, D.Z. Ting, A. Khoshakhlagh, A. Soibel, C.J. Hill, A. Fisher, S. Keo, and S.D. Gunapala, *Appl. Phys. Lett.* 103, 221908 (2013).
3. J.I. Pankove, *Optical Processes in Semiconductors* (New York: Dover Publications, Inc., 1975), pp. 43–44.
4. J.S. Blakemore, *Semiconductor Statistics* (New York: Dover Publications, Inc., 1987).
5. S.E. Schacham and E. Finkman, *J. Appl. Phys.* 57, 2001 (1985).
6. Y.P. Varshni, *Physica* 34, 149 (1967).
7. R. DeWames, P. Maloney, C. Billman, J. Pellegrino, in *SPIE DSS* (2011), vol 8012.

8. L. Hoglund, private communication (IRnova, Kista Sweeden, 2015).
9. M. Abramowitz, I.A. Stegun, ed., *Handbook of Mathematical Functions with Formulas, Graphs and Mathematical Tables*. *National Bureau of Standards Applied Mathematics Series 55*, (Washington, D.C: U.S. Government Printing Office, 1964), pp. 255–272.
10. W. Weiler, *Semiconductors and Semimetals*, Vol. 16 (New York: Academic, 1981).
11. M. Kinch, *State-of-the Art Infrared Detector Technology* (Bellingham: SPIE Press, 2014).
12. S. Maimon and G.W. Wicks, *Appl. Phys. Lett.* 89, 151109 (2006).
13. P. Klipstein, O. Klin, S. Grossman, N. Snapi, B. Yaakobovitz, M. Brumer, I. Lukomsky, D. Aronov, M. Yassen, B. Yofis, A. Glozman, T. Fishman, E. Berkowicz, O. Magen, I. Shtrichman, and E. Weiss, *Proc. SPIE* 7608, 7608IV (2010).
14. J. Schuster, R.E. DeWames, E.A. DeCuir Jr., E. Bellotti, and P.S. Wijewarnasuriya, *Appl. Phys. Lett.* 107, 023502 (2015).
15. J. Schuster, R.E. DeWames, E.A. DeCuir Jr., E. Bellotti, N. Dhar, P.S. Wijewarnasuriya, in *Proceedings of SPIE*, (2015). doi:10.1117/12.2186043.
16. J.P. Rosbeck, R.E. Starr, S.L. Price, and K.J. Riley, *J. Appl. Phys.* 53, 6430–6440 (1982).
17. P.C. Klipstein, *J. Cryst. Growth* 425, 351–356 (2015).